SUPPLEMENTAL FIGURE LEGENDS

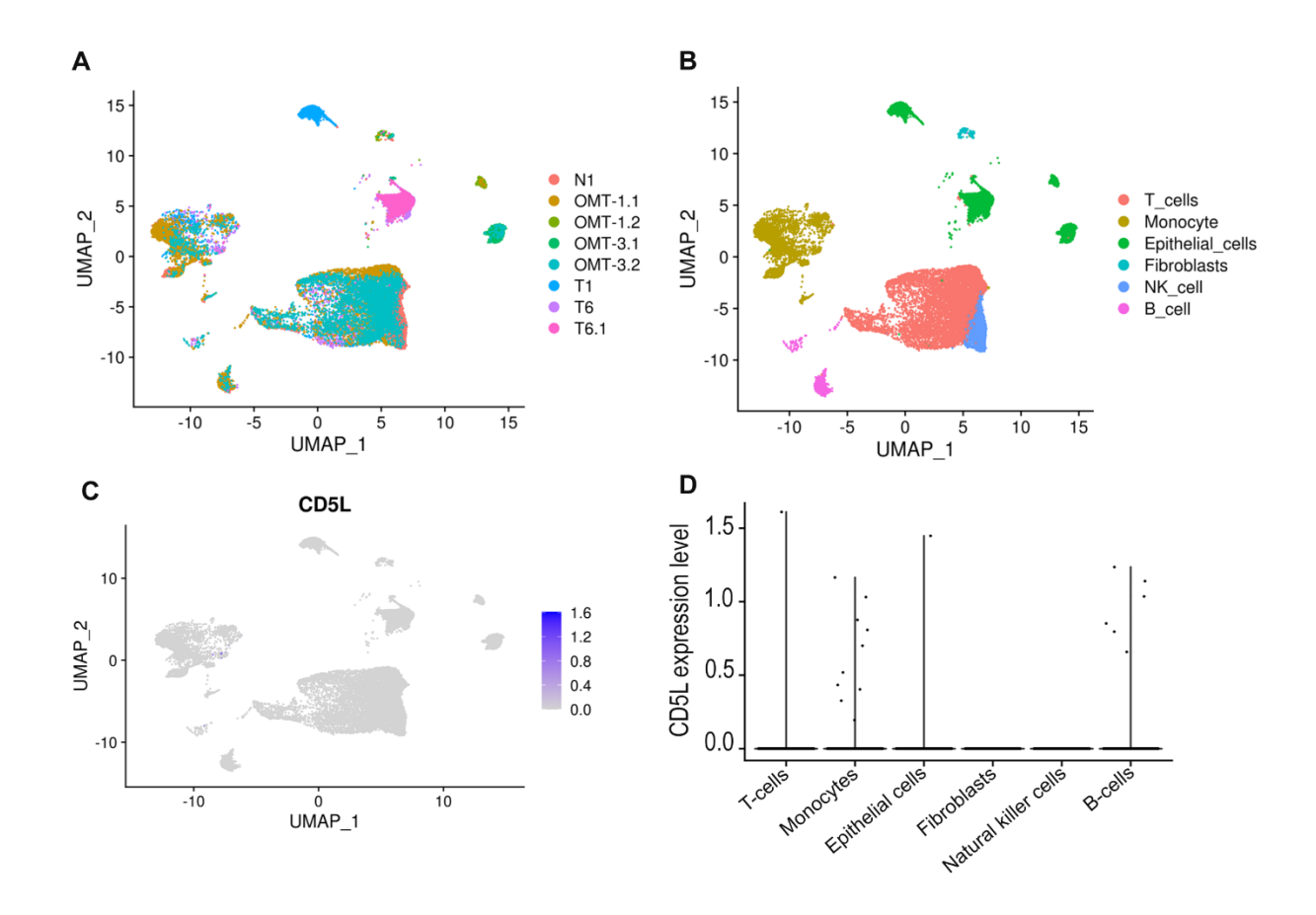


Fig. S1. *CD5L* expression in human ovarian tumors. A total of 5 freshly resected high-grade serous ovarian cancer (HGSC) specimens were collected. Samples were processed using 10X genomic Chromium Single cell 3' v3. UMAP visualization of major cell types was used for subsequent analysis by (A) sample and (B) cell type. (C) UMAP visualization of *CD5L* expression. (D) Violin plot of *CD5L* expression in the major cell types. Samples with similar nomenclature such as OMT-1.1 and OMT-1.2 refers to the same patient which were sorted with CD45+ and CD45- before the single cell analysis. The single cell analysis data was deposited in GEO (Accession number GSE181955).

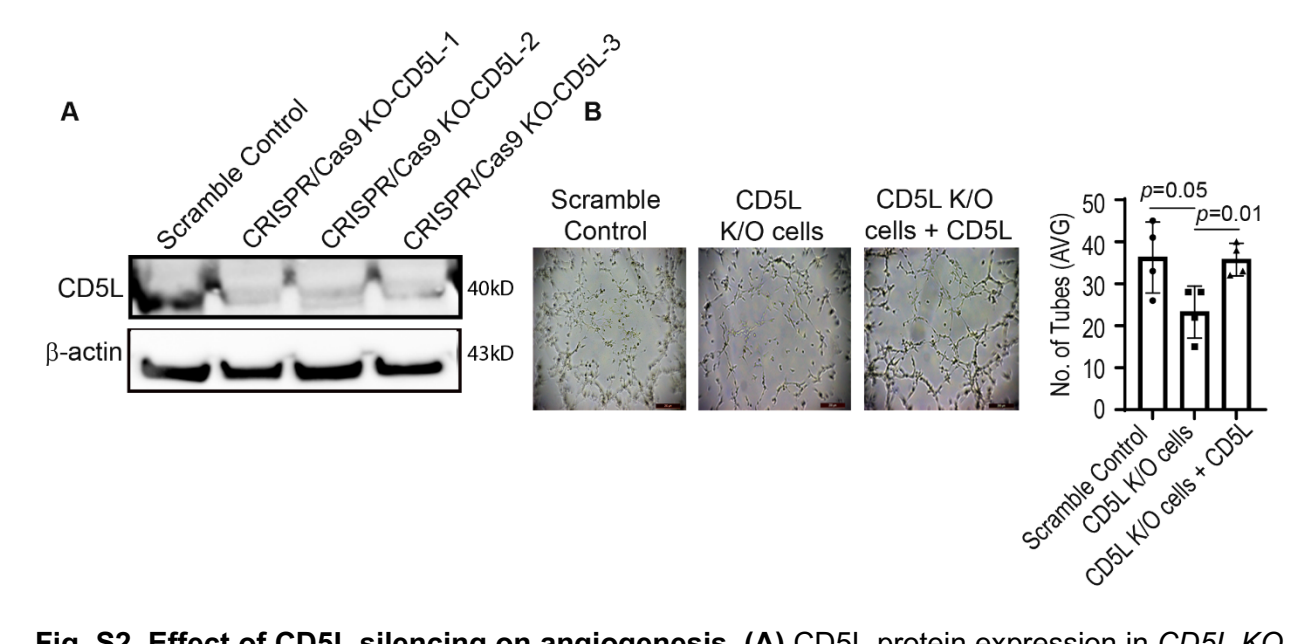


Fig. S2. Effect of CD5L silencing on angiogenesis. (A) CD5L protein expression in *CD5L KO* RF24 cells and (B) tube formation of *CD5L KO* RF24 cells treated with CD5L recombinant protein. Data represented as mean values \pm SD, determined by two-tailed Student 's t test (n = 4 biological independent experiments; scale bar = 200 μ m).

CD5L promoter sequence

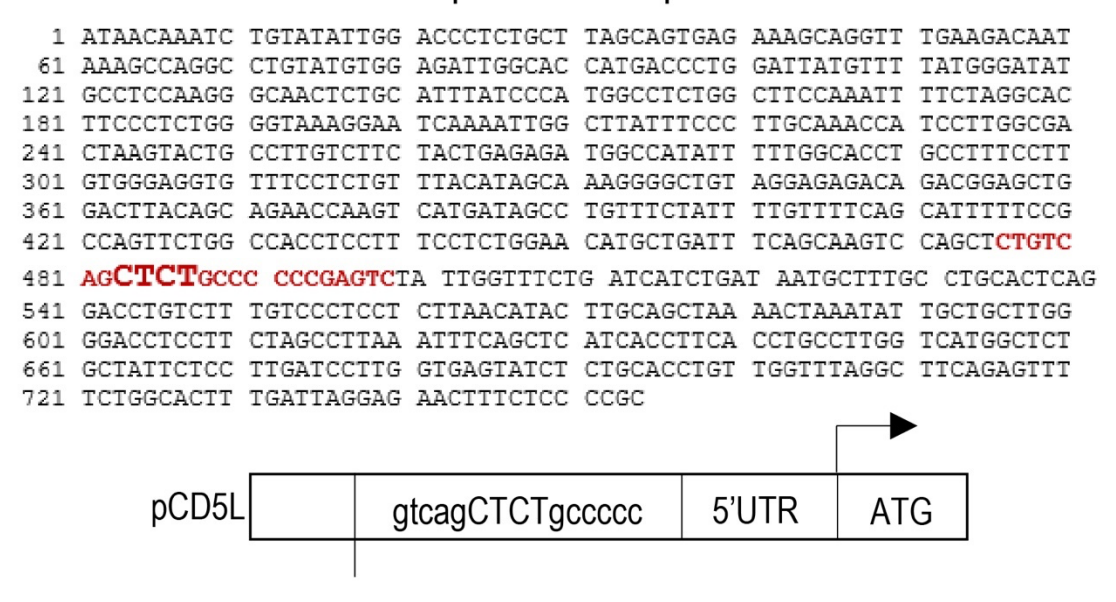


Fig. S3. Promoter sequence of CD5L. PPARG binding site identified in red. Lower image represents *CD5L* promoter construct with critical base pairs in PPARG binding highlighted (CTCT).

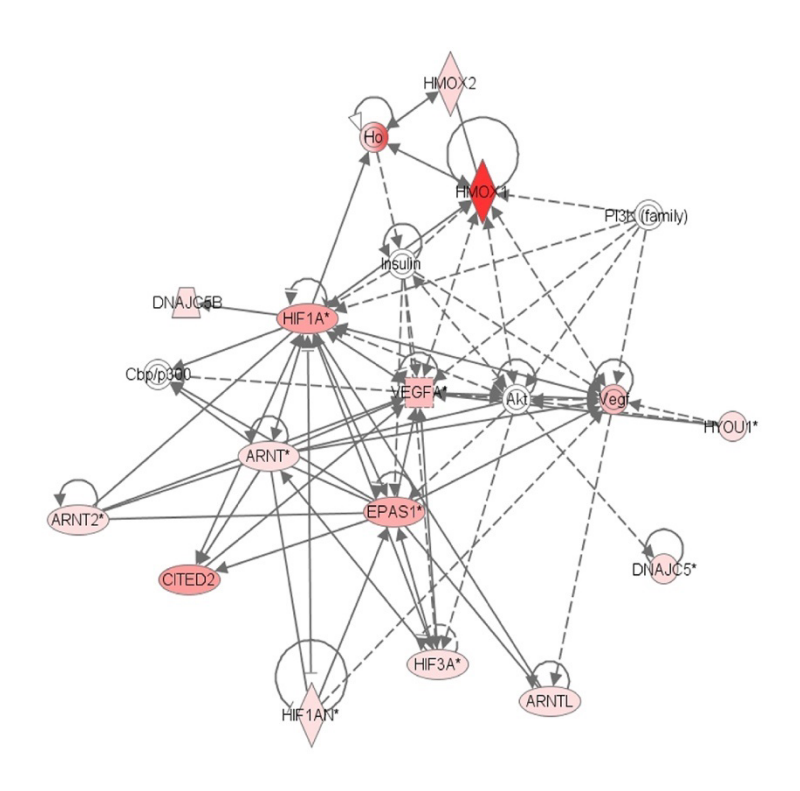


Fig. S4. Ingenuity pathway analysis (IPA) of anti-VEGF antibody (AVA) resistant mouse tumor endothelial cells. Resistance to anti-VEGF therapy is associated with increased hypoxia signaling. IPA analysis performed on gene expression profile presented in Figure 1.

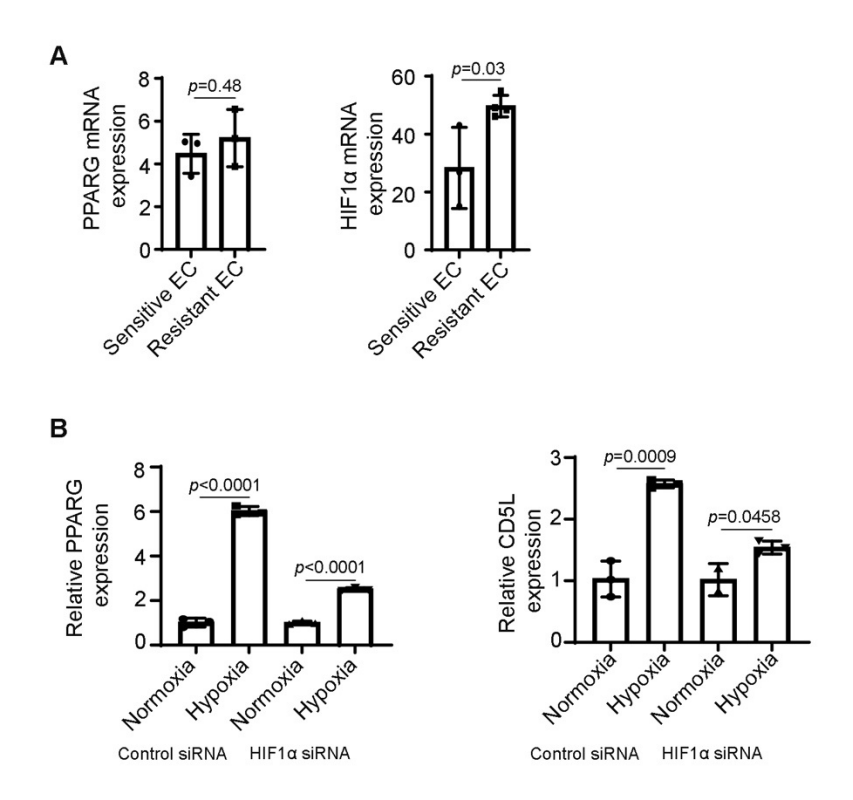


Fig. S5. Upregulation of PPARG and HIF1 α in anti-VEGF antibody-resistant tumor endothelial cells under hypoxic condition. (A) *PPARG* and *HIF1\alpha* expression in B20 sensitive and resistant endothelial cells isolated from SKOV3ip1 ovarian tumor (related to microarray data, Fig. 1A). (B) *PPARG* and *CD5L* expression in RF24 cells treated with *HIF1\alpha* siRNA versus control siRNA in normoxic and hypoxic conditions. Data represented as mean values \pm SD, determined by two-tailed Student 's *t* test (n = 2-3 biologically independent experiments).

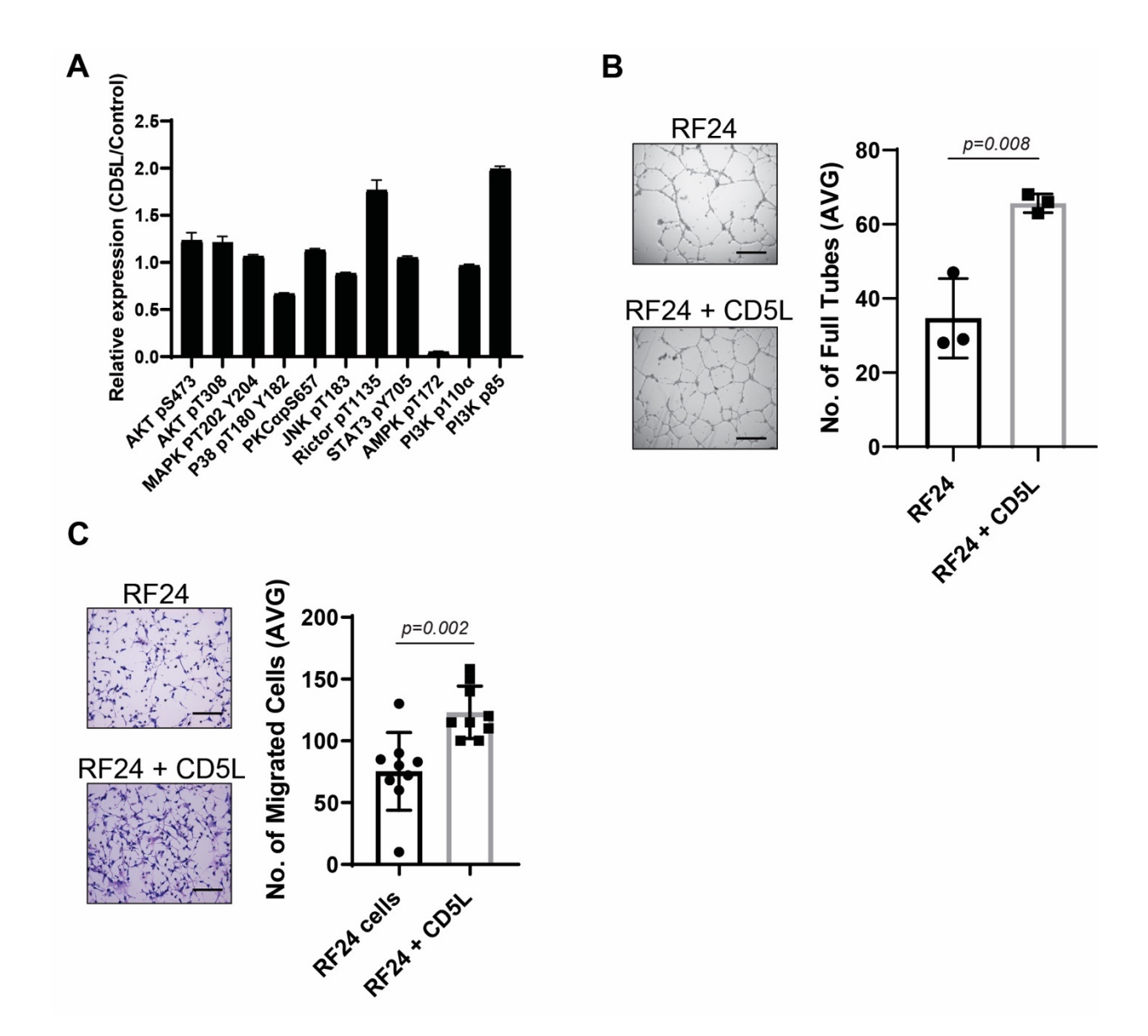


Fig. S6. Effect of exogenous CD5L protein treatment on RF24 endothelial cells. (A) Reverse phase protein array (RPPA) analysis of RF24 endothelial cells treated with CD5L protein *versus* control. (B, C) Tube formation (B) and cell migration (C) of RF24 cells alone or after addition of 400 ng/ml CD5L protein. Data represented as mean values \pm SD, determined by two-tailed Student 's t test (n = 3 biologically independent experiments; scale bar = 500 μ m for B and 200 μ m for C).

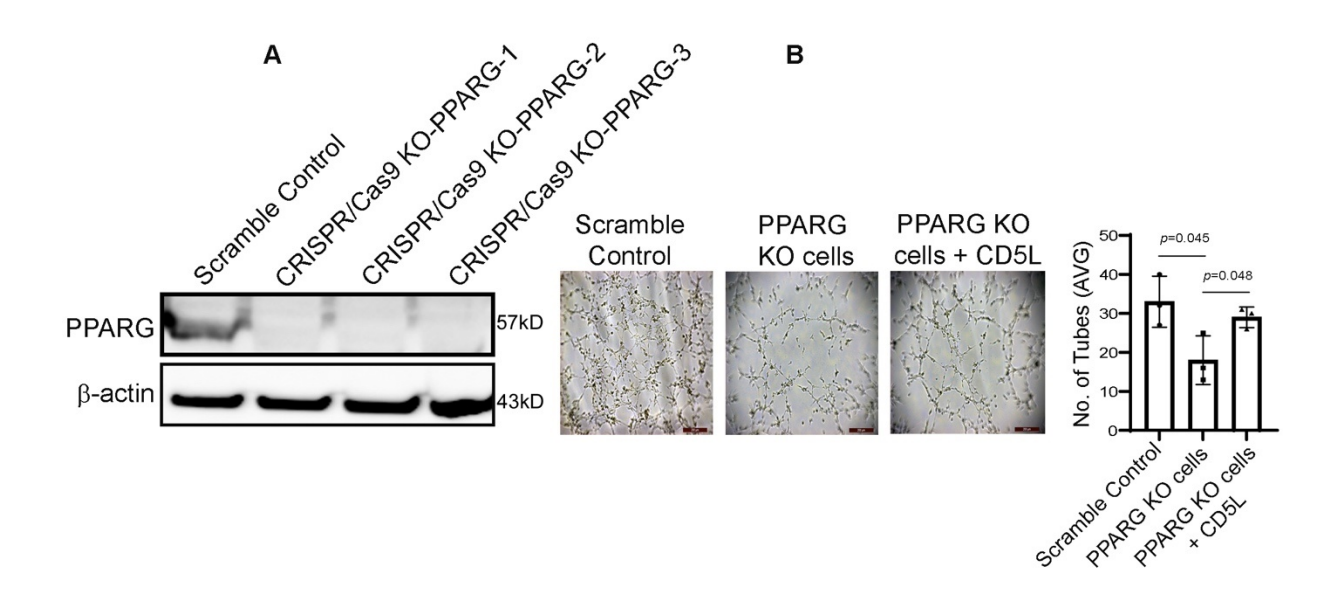


Fig. S7. Effect of PPARG silencing on angiogenesis. (A) PPARG protein expression in PPARG KO RF24 cells and (B) tube formation of PPARG KO RF24 cells treated with CD5L recombinant protein. Data represented as mean values \pm SD, determined by two-tailed Student 's t test (n = 3 biologically independent experiments; scale bar = 200 μ m).

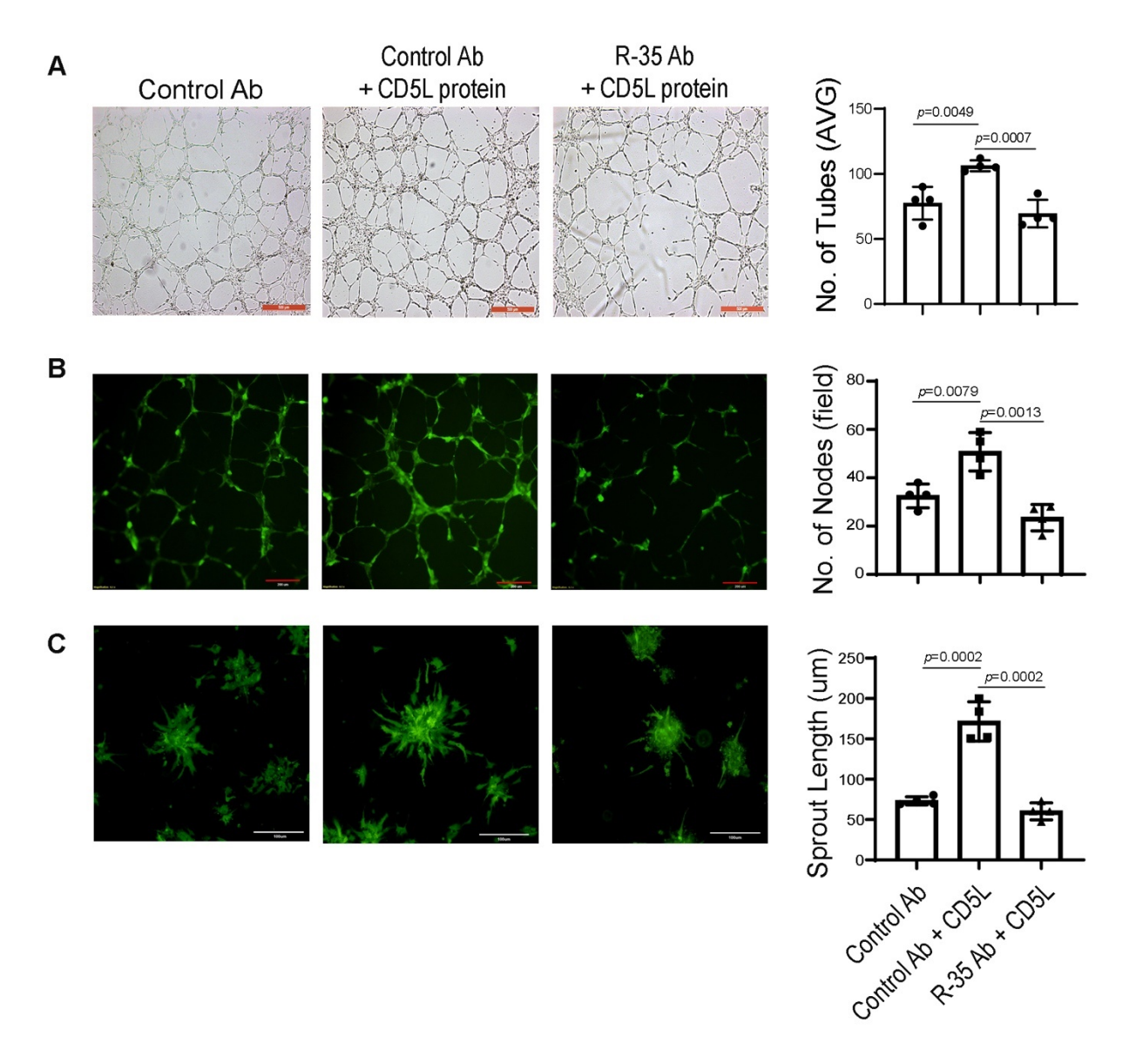
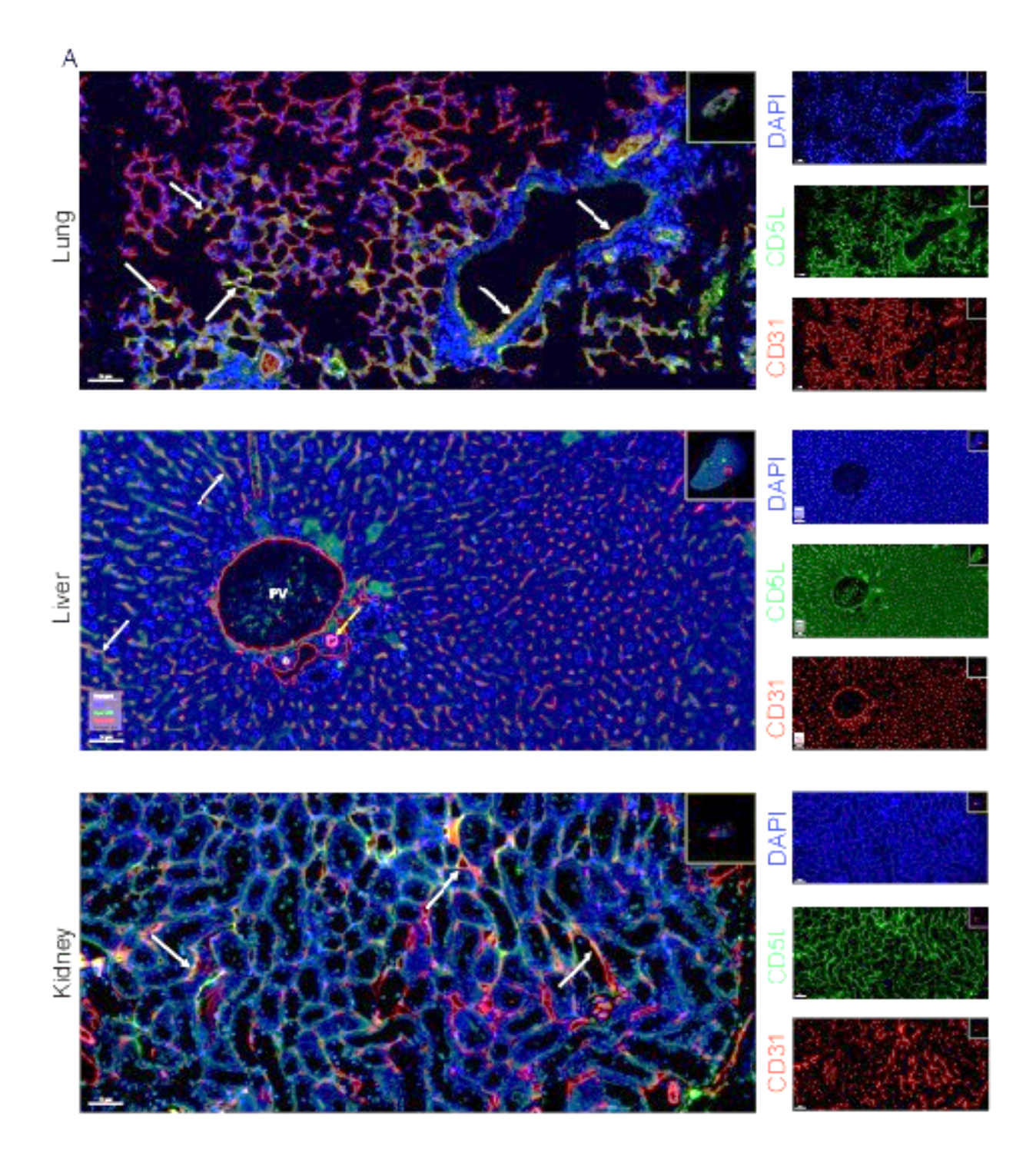


Fig. S8. Effect of CD5L on tube formation and capillary formation. Tube formation of (A) human pulmonary artery endothelial cells (HPAECs; scale bar = $500 \, \mu m$) and (B) human umbilical venous endothelial cells (GFP-HUVECs) treated with CD5L recombinant protein and R-35 antibody; scale bar = $200 \, \mu m$. (C) Capillary formation of GFP-HUVECs treated with CD5L recombinant protein and R-35 antibody (scale bar = $100 \, \mu m$). Data represented as mean values \pm SD, determined by two-tailed Student 's t test (n = 4 biologically independent experiments).



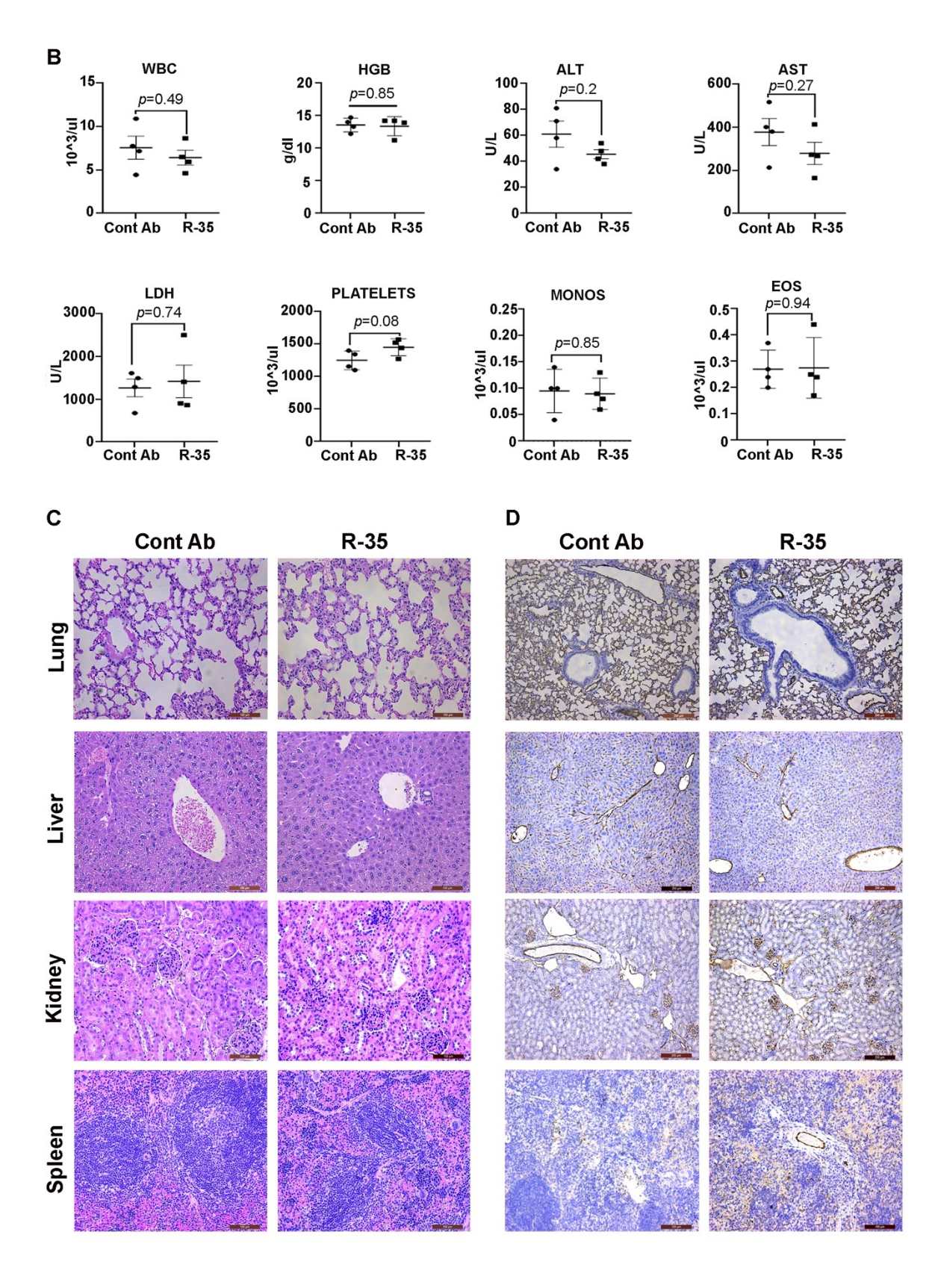


Fig. S9. CD5L expression in lung, liver and kidney endothelial cells and effect of CD5L blocking antibody R-35 on normal mice. (A) Expression of CD5L in endothelial cells of normal organs from C57BL/6 mice (n = 4 mice) - continuous endothelium of lung (white arrows; scale bar = 50 μm); hepatic arterial (denoted by yellow arrow), portal venous (PV), and discontinuous (white arrows; scale bar = 50 μm) endothelium in liver; capillary epithelium of kidney (white arrows and scale bar = 50 μm). (B) Serum levels of white blood cells (WBC), hemoglobin (HGB), aspartate aminotransferase (AST), alanine aminotransferase (ALT), lactate dehydrogenase (LDH), platelets, monocytes (MONOS), and eosinophils (EOS) in normal C57BL/6 mice treated with either control antibody or R-35 antibody. (C) Hematoxylin and eosin (H&E) staining of lung, liver, kidney, and spleen of normal C57BL/6 mice treated with either control antibody or R-35 antibody. (D) CD31 staining of endothelial cells of normal C57BL/6 mice treated with either control antibody or R-35 antibody. Data represented as mean values \pm SEM, determined by two-tailed Student 's *t* test (n = 4 biologically independent experiments for B, C and D. Scale bar = 100 μm for both C and D).

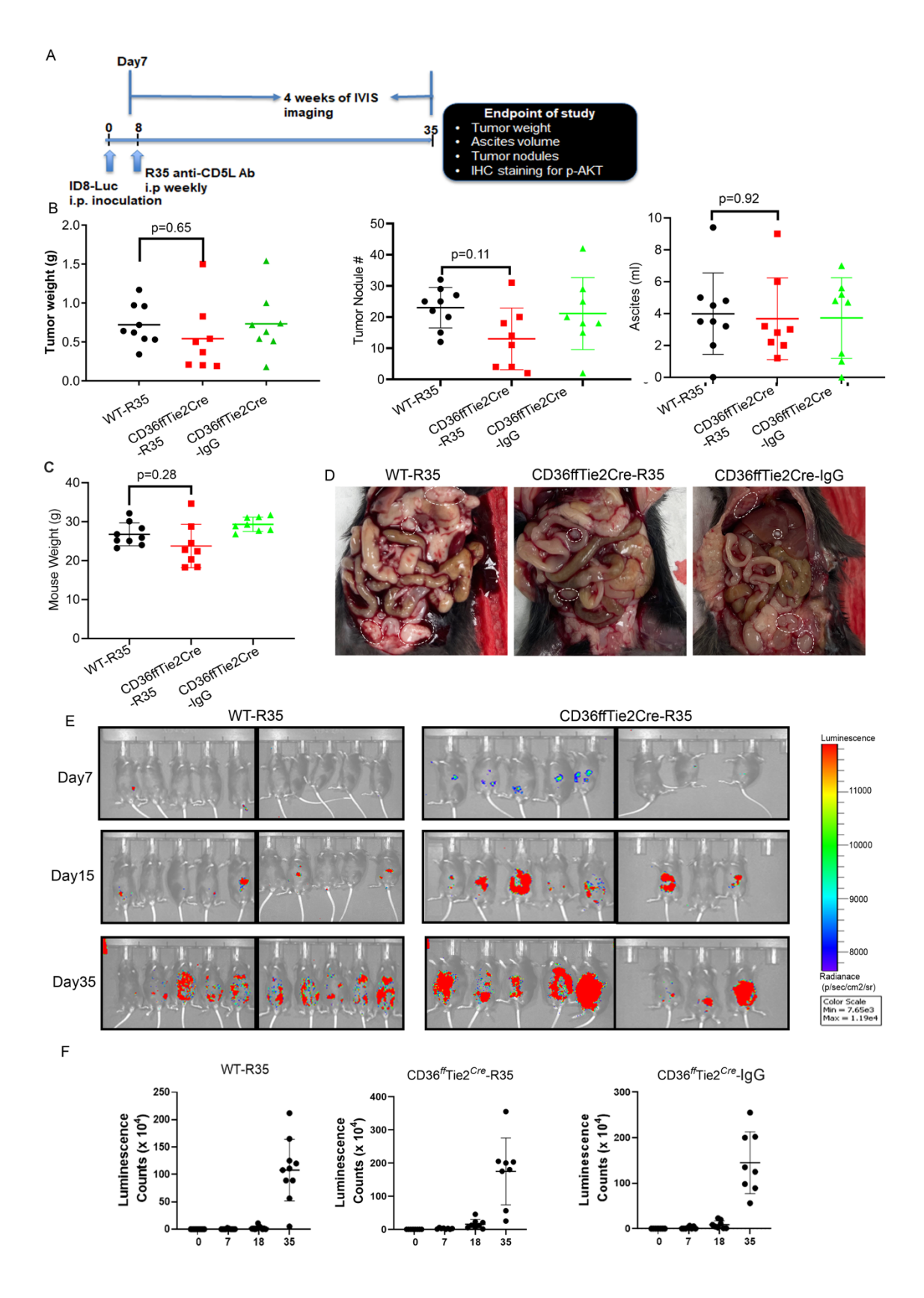


Fig. S10. *In vivo* study of anti-CD5L-antibody (R-35) therapeutic effect on syngeneic ovarian cancer models using endothelial-specific *CD36* knockout (CD36^{flox/flox} Tie2^{cre}) strain. (A) Mice from the CD36^{flox/flox} Tie2^{cre} model were treated with anti-CD5L antibody (R-35) after inoculation with ID8 cells labeled with luciferase. (B) Tumor weight, number of tumor nodules, and volume of ascites fluid. (C) Body weight of each mouse recorded at the time of necropsy. Data represented as mean values ± SD determined by two-tailed nonparametric Student's *t* test (n = 9 for WT-R35; n = 8 for CD36^{flox/flox}Tie2^{cre}-R35 and CD36^{flox/flox}Tie2^{cre}-IgG groups, respectively). (D) Representative gross images from C57BL/6, CD36^{flox/flox}Tie2^{Cre} mice that received R-35 or control IgG antibody treatment. (E) Gross images for bioluminescence in C57BL/6 or CD36^{flox/flox}Tie2^{Cre} mice. (F) Quantification of bioluminescence imaging for the three groups of mice.

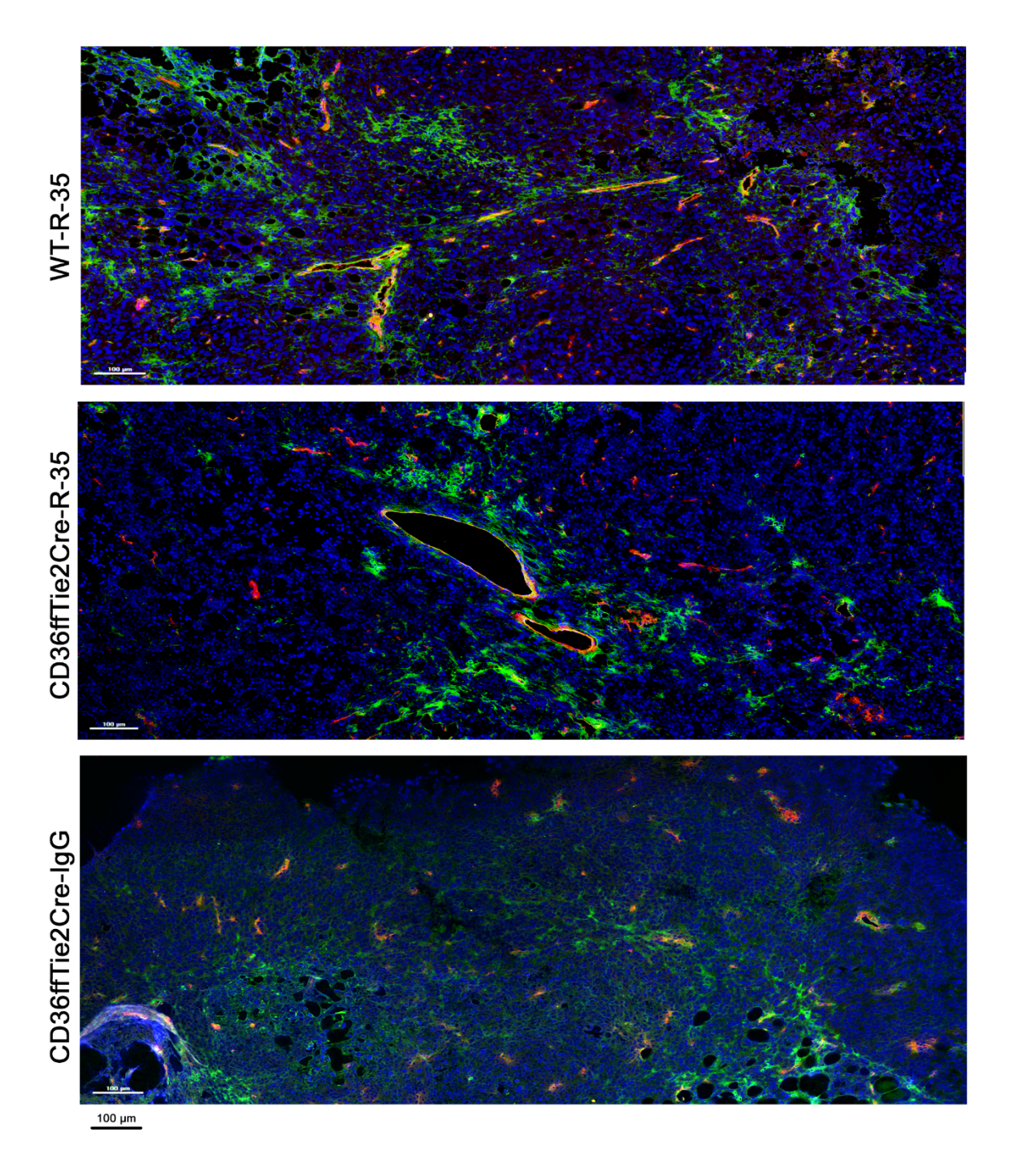


Fig. S11. Effects of anti-CD5L antibody (R-35) on angiogenesis in endothelial-specific *CD36* knockout ID8 tumors. CD31(Red) and pAKT (Green) immunofluorescence staining of tumors from CD36 endothelial-specific KO mice treated with R-35 antibody or IgG (n = 4 biologically independent experiments; scale bar = $100 \mu m$).

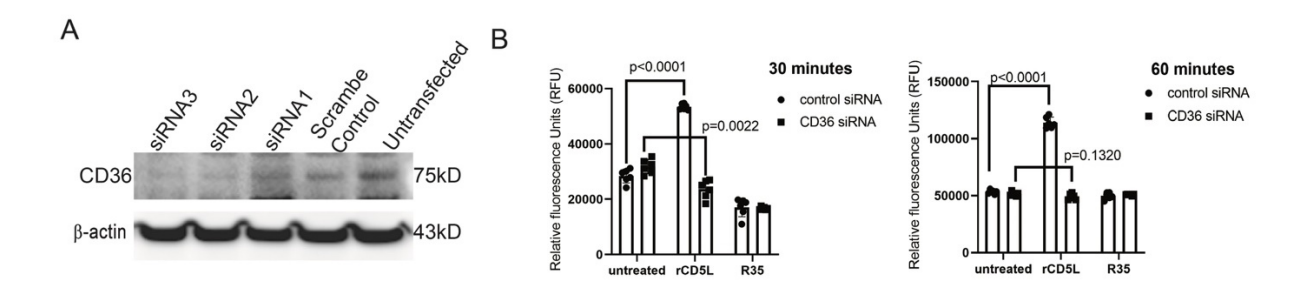


Fig. S12. Fatty acid uptake in RF24 cells with CD5L stimulation or CD36 knockdown. (A) CD36 protein expression in RF24 cells treated with human CD36 siRNA *versus* control siRNA. (B) Relative exogenous fatty acid uptake in RF24 cells treated with control, rCD5L, anti-CD5L antibody (R-35) after serum starvation for 30 min and 60 min and supplementation with fluorescently labeled dodecanoic acid. Data represented as mean values \pm SD determined by two-tailed Student 's t test (n = 6 biological independent experiments).

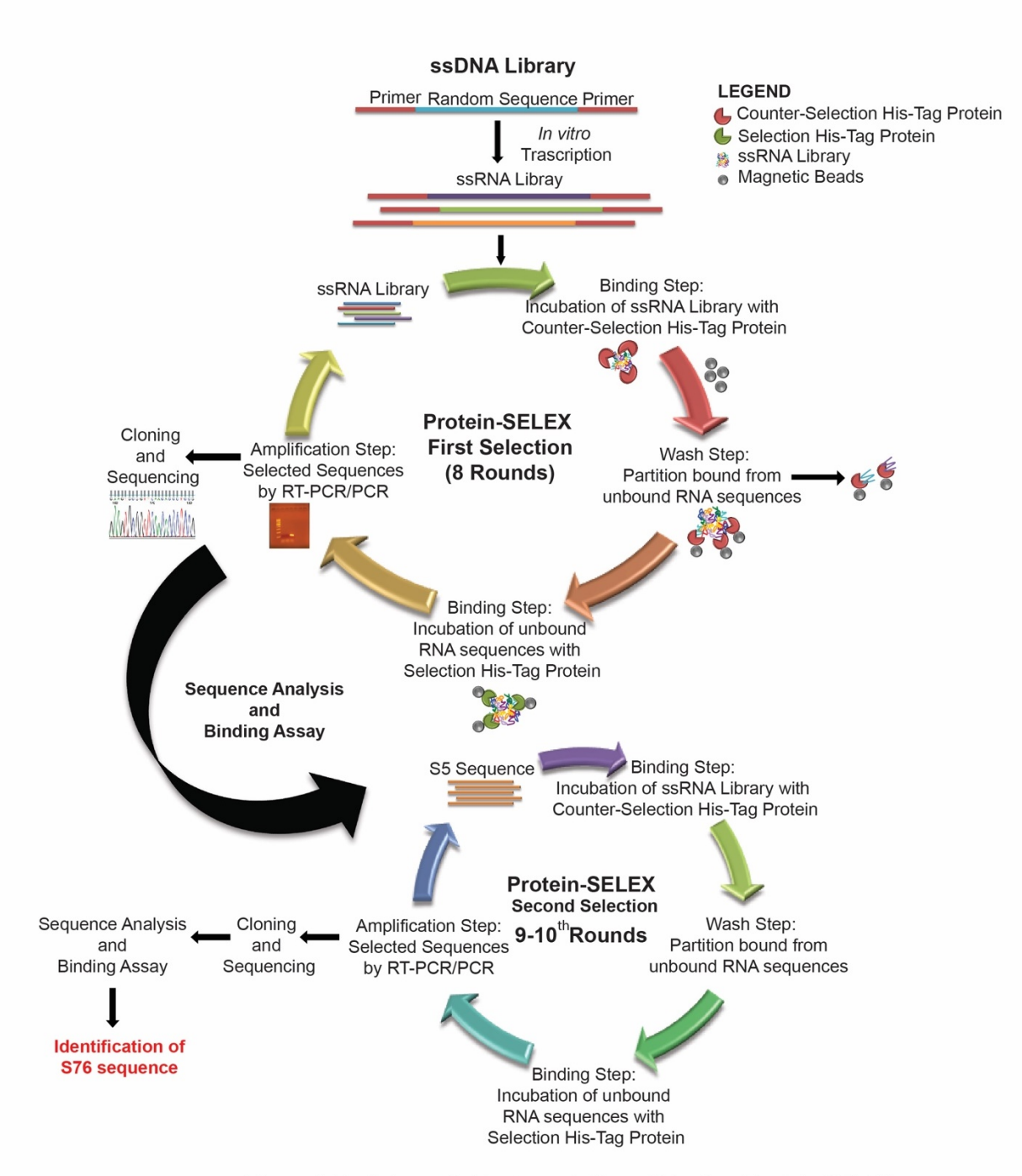


Figure S13. Schematic Representation of Tandem Protein-SELEX

Fig. S13. Schematic Representation of Tandem Protein-SELEX. S76.T selection by the tandem protein-SELEX method.

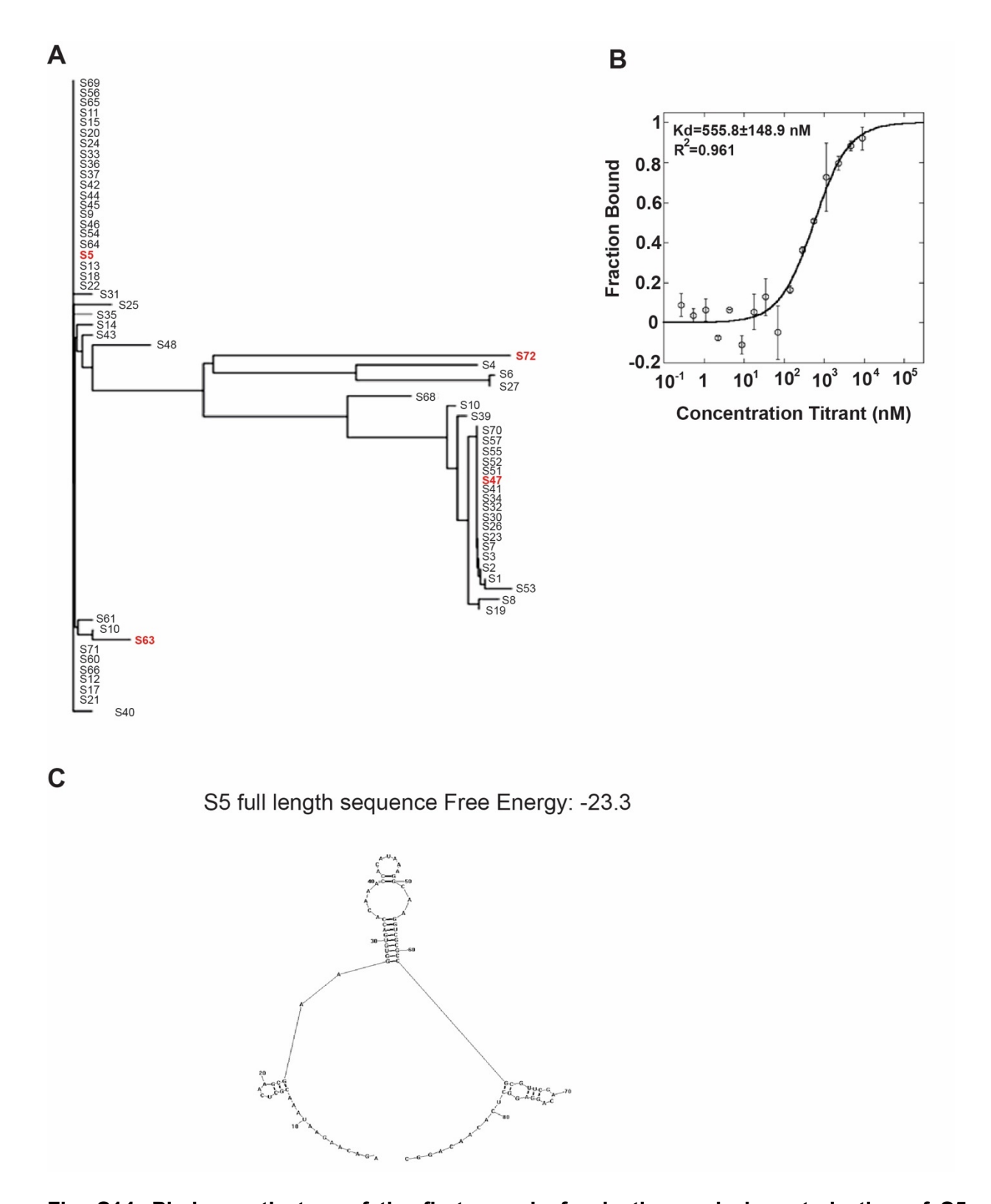


Fig. S14. Phylogenetic tree of the first round of selection and characterization of S5 sequence. (A) Phylogenetic tree generated by using ClustalW2 software and visualized with

TreeVieX program. **(B)** S5 sequence binding curve obtained by microscale thermophoresis (MST). Data represented as mean values \pm SD (n = 2 biologically independent experiments). **(C)** Secondary structure prediction of S5 sequence by using RNA structure version 5.1.

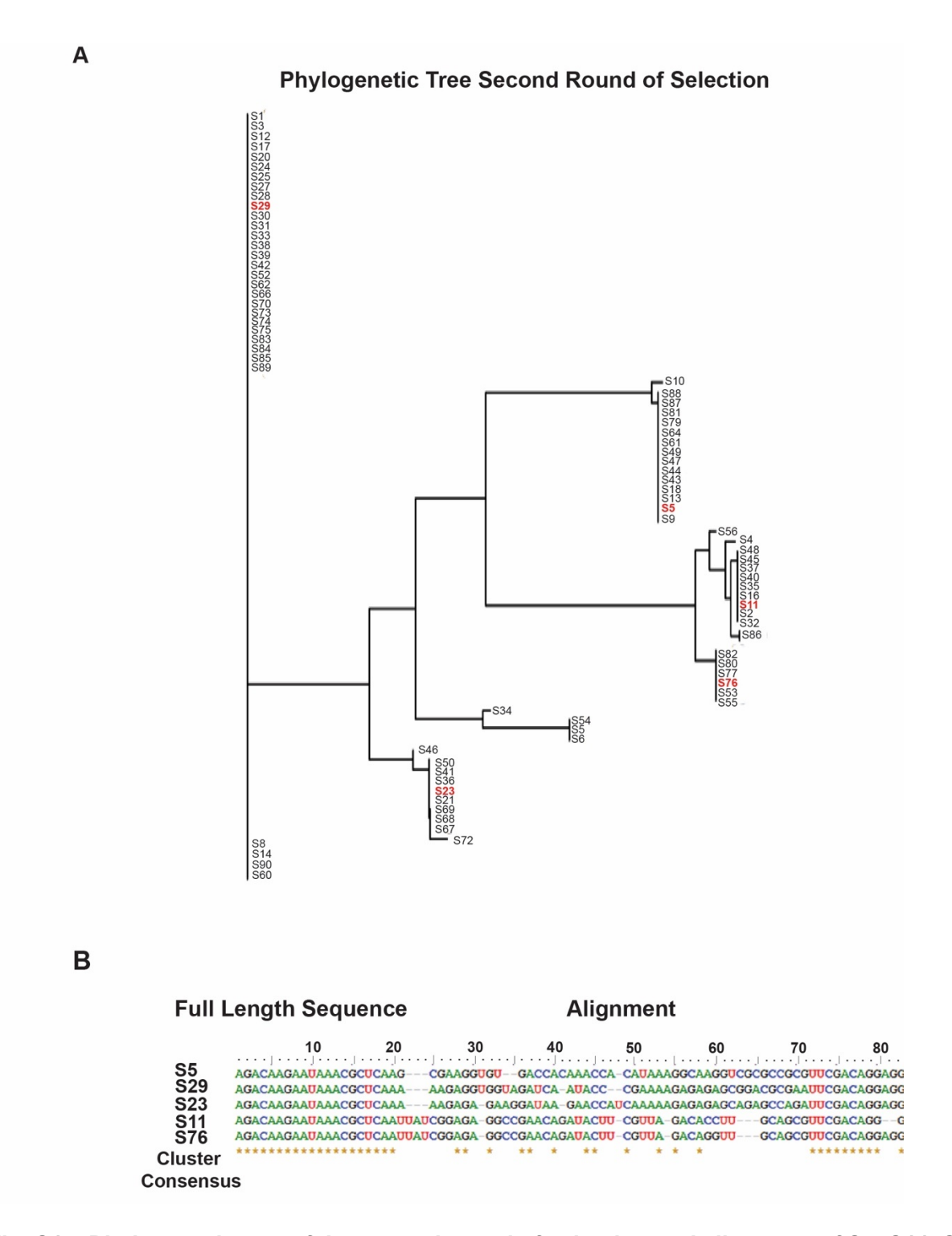


Fig. S15. Phylogenetic tree of the second round of selection and alignment of S5, S11, S23, S29, and S76 sequences. (A) Phylogenetic tree of second round of tandem protein-SELEX. (B) Alignment of S5, S11, S23, S29, and S76 sequence.

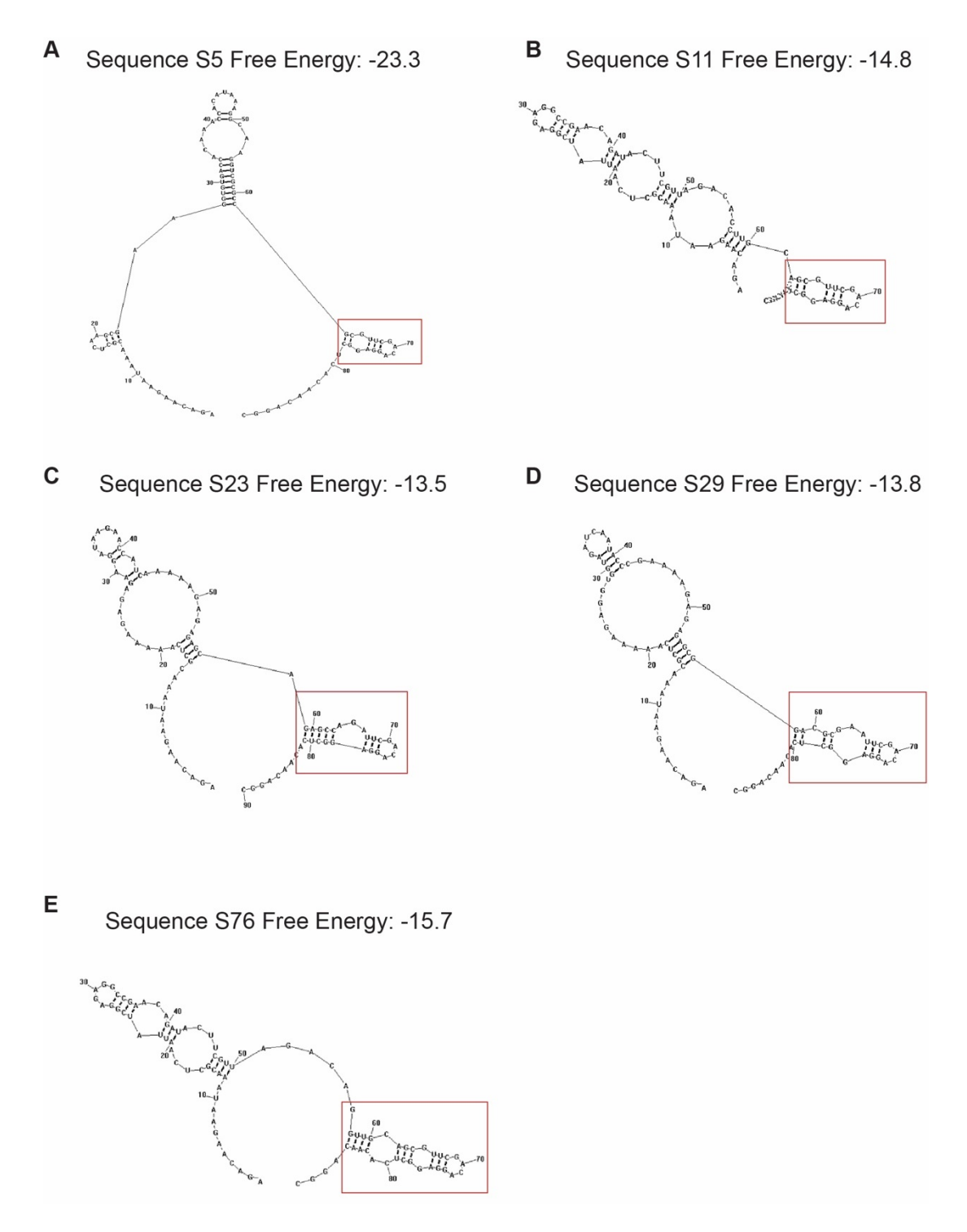


Fig. S16. Identification of binding site for S11, S23, S29, and S76. Prediction of secondary structure of S5 **(A)**, S11 **(B)**, S23 **(C)**, S29 **(D)**, and S76 **(E)** sequences to identify the functional part of the aptamer involved in the recognition of CD5L target.

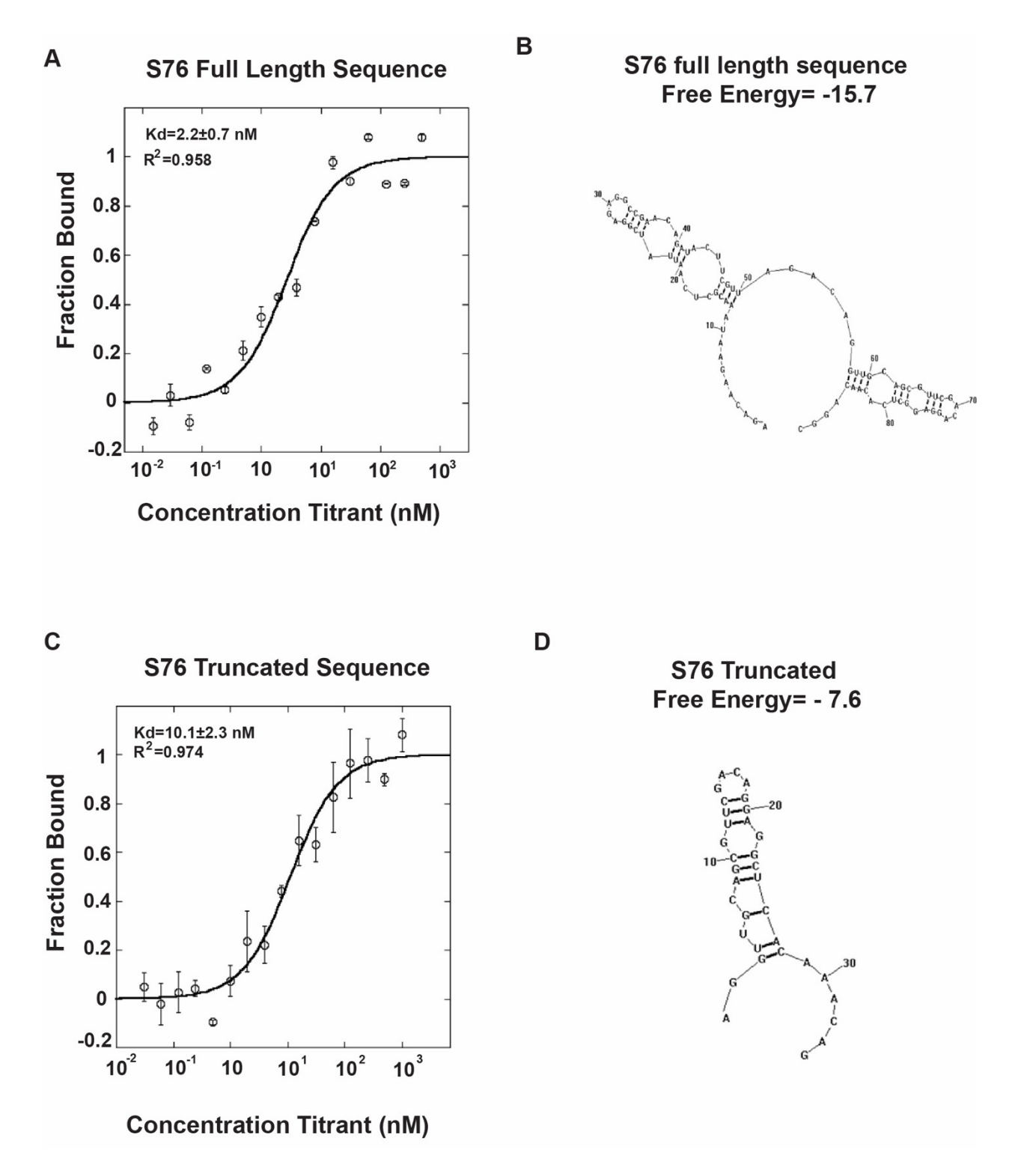


Fig. S17. Comparison of binding affinity and secondary structure of S76 and S76.T. (A, B) Binding affinity (A) of full-length S76 sequence by MST and prediction of secondary structure (B) by using RNA structure version 5.1. (C, D) Binding affinity (C) of truncated S76 (S76.T) sequence

by MTS and prediction of secondary structure (D) by using RNA structure version 5.1. For A and C, data represented as mean values \pm SD (n = 2 biologically independent experiments).

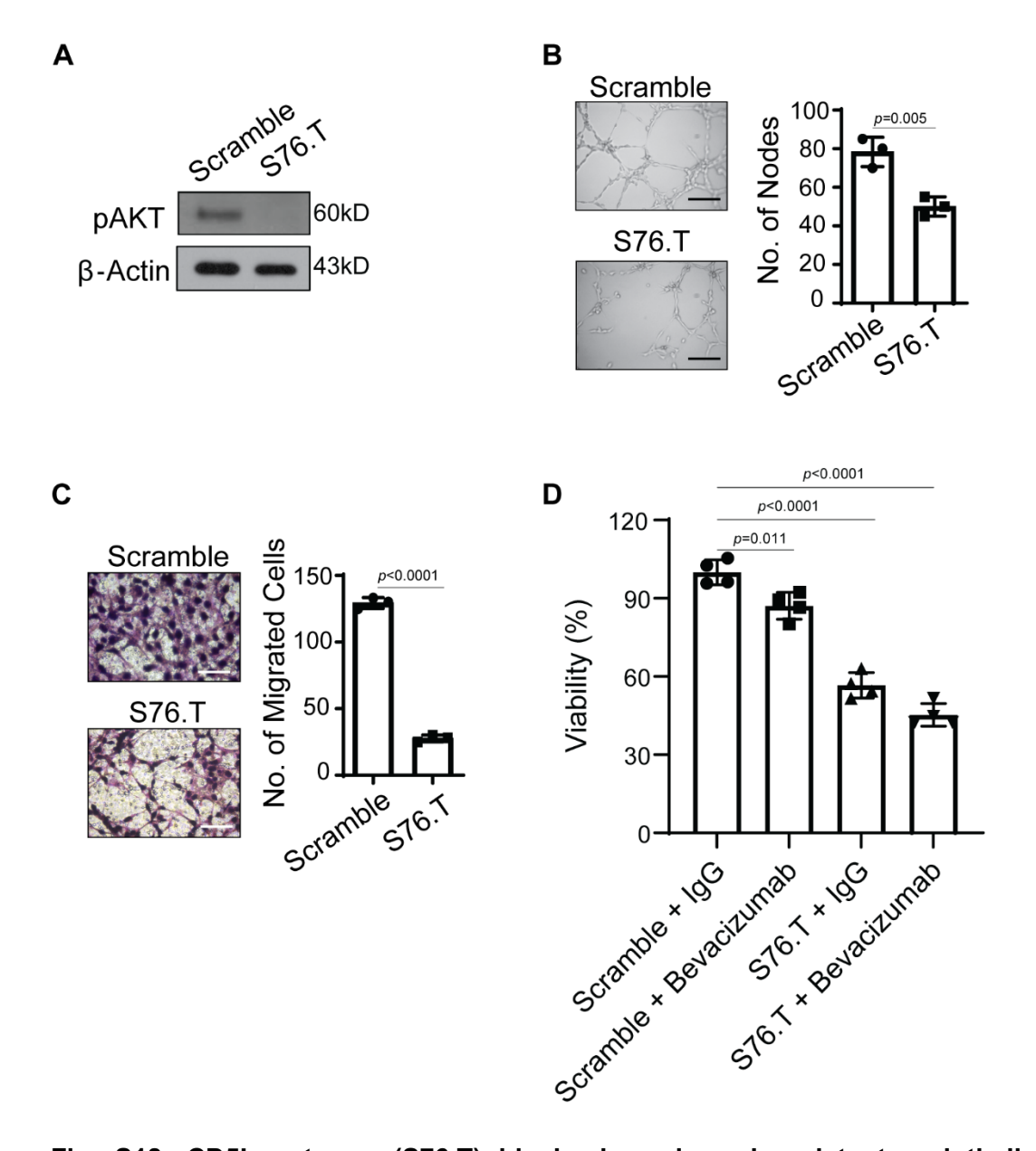


Fig. S18. CD5L aptamer (S76.T) blocks bevacizumab-resistant endothelial cells. (A) Expression of pAKT in bevacizumab-resistant RF24 cells after treatment with the S76.T-aptamer. (B, C) S76.T-aptamer significantly reduces tube formation (B) and cell migration (C) compared with scramble aptamer in bevacizumab-resistant RF24 cells (scale bar = 200 μ m for both B and C). (D) Cell viability assay in RF24 endothelial cells. RF24 endothelial cells were treated with S76.T-aptamer alone or in combination with bevacizumab. Data represented as mean values \pm SD, determined by two-tailed Student 's t test except one-way Anova Tukey's multiple comparisons for D (n = 3 biologically independent experiments for B, C and n = 4 biologically

independent experiments for D).

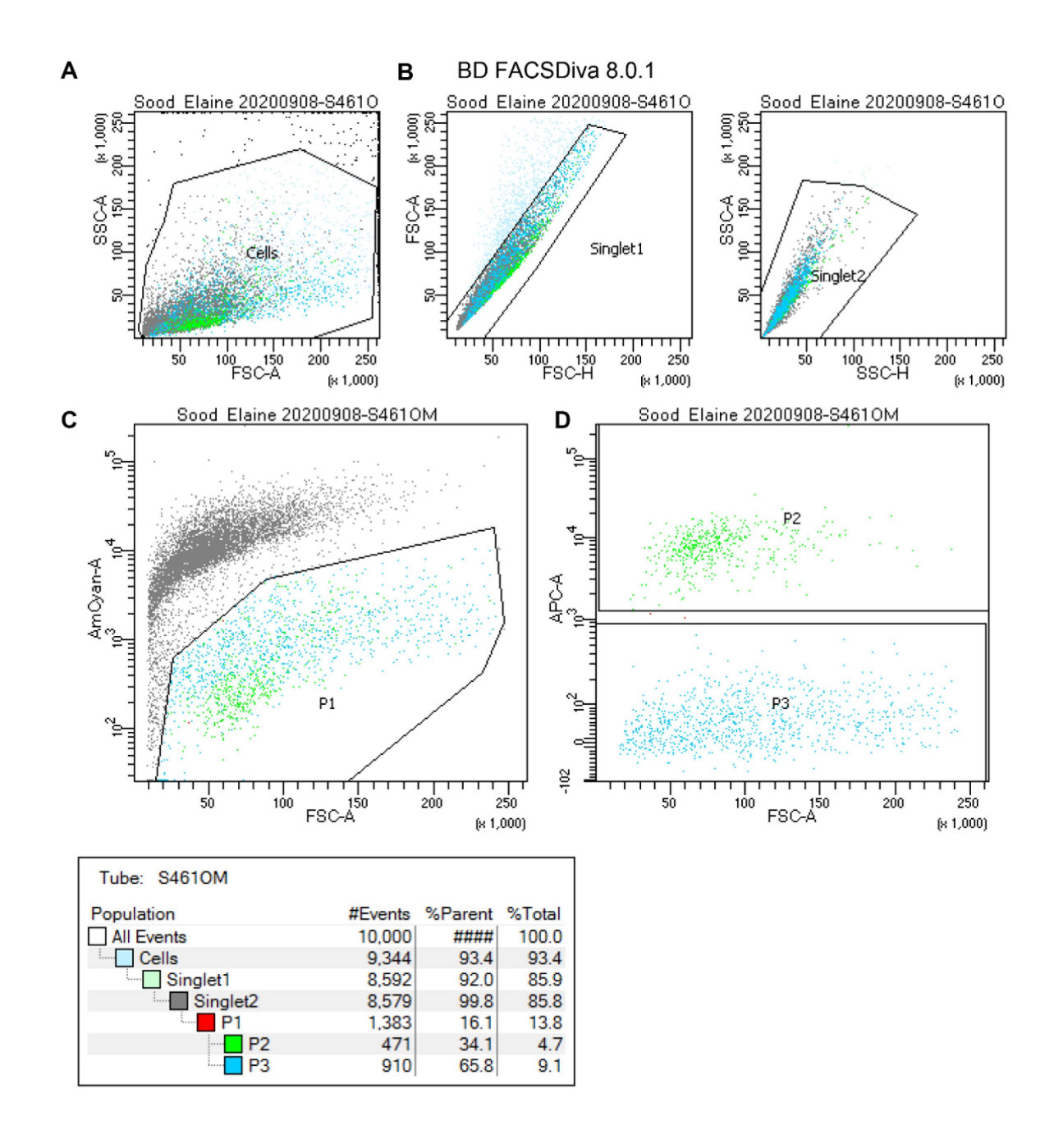


Fig. S19. Representative example of gating strategy for cell sorting applied in single-cell analysis. Cells were first gated by A) All cells; B) single cells / singlets, followed by the cell viability dye; C) where only live cells were gated (AmCyan and FSC-A); and (D) cells were sorted and collected by CD45 positive and CD45 negative cells (APC and FSC-A).

Supplementary Table 1. Kd Binding Values for S5, S47, S63 and S72 Obtained by MTS

Sequence Name	Kd vs CDL5	Kd vs VEGF
S5	555.8±148.9 nM	Weak binding, not fit with the law of mass action
S47	1552.4±309.4 nM	103.4±45.4 nM
S63	No binding between 500 pM to 50 mM	Weak binding, not fit with the law of mass action
S72	Weak binding, not fit with the law of mass action	135.2±61.6 nM

Supplementary Table 2. Kd Binding Values for S11, S23 and S76 Obtained by MTS

Sequence Name	Kd vs CDL5	Kd vs VEGF
S11	59.2±22.14 nM	Weak binding, not fit with the law of mass action
S23	92.1±40.1 nM	Weak binding, not fit with the law of mass action
S76	2.2±0.7 nM	Weak binding, not fit with the law of mass action

Supplementary Table 3. Quantitative-PCR primer lists

No.	Primers	Sequence (5'-3')
1	Human CD5L F	5'- CTGCTTGTTCTCCTGAGCCC -3'
2	Human CD5L R	5'- TCAAAGGGTCAGGGTTGAGC -3'
3	Human PPAR-γ F	5'- GCCCTTTGGTGACTTTATGGA -3'
4	Human PPAR-γ R	5'- GCAGCAGGTTGTCTTGGATG -3'
5	Human CD36 F	5'- GAGAACTGTTATGGGGCTAT -3'
6	Human CD36 R	5'- TTCAACTGGAGAGGCAAAGG -3'
7	Tie2 Cre transgene F	5'-CGCATAACCAGTGAAACAGCATTGC-3'
8	Tie2 Cre transgene R	5'-CCCTGTGCTCAGACAGAAATGAGA-3'

Supplemental Table 4. Materials used

Reagent or resource	Source	Identifier		
Experimental mod	Experimental models: cell lines			
SKOV3ip1	MDA Cell Line Core	CVCL_0C84		
ID8	Dr. Roby at Univ. of Kansas	CVCL_IU14		
RF24	ABM (Applied Biological Materials)	CVCL_AX74		
HEK293T	ATCC	CVCL_0063		
HPAEC	ATCC	N/A		
HUVEC-GFP	ANGIO-PROTEOMIE	CAP-0001GFP		
Experimental mod	dels: organisms/strains			
Mouse: PPARG ^{ft/fl} ;Tie ²⁻ Cre ^{+/-} female and male	Dr. Yihong Wan, University of Texas Southwestern (10 mice/group)	N/A		
Mouse: Female athymic nude mice (NCr-nu)	Taconic (10 mice/group)	N/A		
Chemicals, peptid	les, and recombinant proteins			
Optimal Cutting Temperature (OCT) media	Miles, Inc., Elkhart, IN	Catalog no. 25608- 930		
RNeasy mini kit	Qiagen, Hilden, Germany	Catalog no. 74104		
SYBR Green ER qPCR SuperMix Universal	Invitrogen, Carlsbad, CA	Catalog no. 4368708		
siRNAs	Sigma-Aldrich, St. Louis, MO	Universal negative control; SIC001 CD5L: SASI_Hs02_0034049 4 PPARG: SASI_Hs01_0010649 8		
Lipofectamine 2000	Invitrogen	Catalog no. 11668027		
LY294002	Selleckchem, Houston, TX	Catalog no. S1105		
Topotecan	Sigma-Aldrich	123948-87-8		

YC-1	Sigma-Aldrich	170632-47-0	
Cobalt Chloride, CoCl ₂	Sigma-Aldrich	7646-79-9	
Human recombinant CD5L protein	Sino Biological, Beijing, China	Catalog no. 10791- H08H	
Bevacizumab	Genentech, South San Francisco, CA	N/A	
MTT reagent	Sigma-Aldrich	Catalog no. M2128	
Aptamer	Sigma-Aldrich	N/A	
His-tagged VEGF-A	Abnova, Taiwan	Catalog no. P5816	
His-tagged CD19	Life Technologies, Carlsbad, CA	Catalog no. 11880H08H250	
6-His Peptide tagged	BioLegend, San Diego, CA	Catalog no. 931601	
DNA library	TriLink Biotechnologies, San Diego, CA	Fitzwater T. and Polisky B. (1996)	
M-MuLV Reverse Transcriptase	Roche, Indianapolis, IN	Catalog no. 11062603001	
Ni ²⁺ NTA Magnetic Agarose Beads	Qiagen	Catalog no. 36111	
TRIzol Reagent	Life Technologies	Catalog no. 15596026	
TOPO Cloning	Life Technologies	Catalog no. K4500- 01SC, K4550-01SC, K4600-01SC	
Antibodies: Expre resin to >95% pur	essed in HEK293 suspension cells and purified with us ity.	se of protein A affinity	
CD31	Cell Signaling Technologies, Beverly, MA	Catalog no. 77699, RRID:AB_2722705 (1:100 dilution)	
PE-CD31	BD Biosciences, San Jose, CA	Catalog no. 555446, RRID:AB_395839 (1:200 dilution)	
CD31	Pharmingen, San Diego, CA	Catalog no. 557355, RRID:AB_396660 (1:800 dilution)	
Ki67	Neomarkers, Fremont, CA	Catalog no. RM-9106- R7, RRID:AB_149920 (1:200 dilution)	

AKT	Cell Signaling Technologies	Catalog no. 4691, RRID:AB_915783 Catalog no. 9272, RRID:AB_329827; (1:1000 dilution)
Phospho-AKT	Cell Signaling Technologies	Catalog no. 4060, RRID:AB_2315049 (1:000 dilution)
Phospho-AKT	Abcam, Cambridge, MA	Catalog no. ab81283 RRID:AB_2224551 (1:50 dilution)
PPARG	Cell Signaling Technologies	Catalog no. 2430, RRID:AB_823599 (1:200 dilution)
PPARG	Abcam	Catalog no. ab59256, RRID:AB_944767 (1:1000 dilution)
HIF1α	Thermo Fisher Scientific, Waltham, MA	Catalog no. MA1-516, RRID:AB_325431 (1:1000 dilution)
CD5L (AIM)	Santa Cruz Biotechnology, Santa Cruz, CA R&D Systems, Minneapolis, MN	Catalog no. sc- 514281; RRID:AB_2076351 (1:1000 dilution)
CD5L (AIM)	Invitrogen, Carlsbad, CA	Catalog no. 703558, RRID:AB_2762393 (1:200 dilution)
CD5L (AIM)	R&D Systems, Minneapolis, MN	Catalog no. AF2797, RRID:AB_2076351 (1:500 dilution)
CD5L (AIM)	Thermo Fisher Scientific, Waltham, MA	Catalog no. PA5- 84779, RRID:AB_2791929 (0.04-0.4 µg/mL)
CD36	Abcam, Cambridge, MA	Catalog no. ab252922 (1:1000 dilution)
β-actin	Sigma-Aldrich	Catalog no. A5441, RRID:AB_476744 (1:5000 dilution)
Vinculin	Sigma-Aldrich	Catalog no. V9131, RRID:AB_477629 (1:2000 dilution)
Anti-rabbit secondary	Sigma-Aldrich	Catalog no. NA934, RRID:AB_772206

antibodies conjugated with horseradish peroxidase. Anti-mouse secondary antibodies conjugated with horseradish peroxidase.	Sigma-Aldrich	(1:2000 dilution) Catalog no. NA931, RRID:AB_772210 (1:2000 dilution)
pLenti-C- mGFP-human CD5L vector	OriGene, Rockville, MD	Catalog no. RC206528L2
Critical commerci	al assays	
Click-iT EdU Assay Kit	Invitrogen	Catalog no. C10632
CD5L ELISA Kit	Mybiosource, San Diego, CA, USA	Catalog no. MBS2024653
Verso cDNA kit	Thermo Scientific	Catalog no. AB1453B
RNeasy mini kit	Qiagen	Catalog no. 74106
EZ ChIP™ kit	Millipore, Temecula, CA	Catalog no. 17-371
Software and algo	orithms	
GraphPad Prism 7.0.	GraphPad Prism 7.0.	GraphPad Software, La Jolla, CA
Windows statistical software	SPSS version 12 for Windows statistical software	SPSS, Inc., Chicago, IL
R statistical package	R.3.4.1	R Foundation for Statistical Computing, Vienna, Austria
ImageJ	ImageJ 1.52a	Wayne Rasband, National Institutes of Health, Bethesda, MD
ClustalW2 software	http://bonsai.hgc.jp/~mdehoon/software/cluster/software.h tm	de Hoon M.J. Imoto S. Nolan J. Miyano S. Open source clustering software. Bioinformatics. 2004; 20: 1453-1454
TreeViewX	http://jtreeview.sourceforge.net/	Saldanha A.J.

program		Java extensible	Treeview
		visualization microarray o	
		Bioinformati 20: 3246-32	-
Monolith NT.115	NanoTemper Technologies GmbH, Munich, Germany	Stoltenburg PLoS One.	